Letter

Mirror-protected Majorana zero modes in f-wave multilayer graphene superconductors

Võ Tiến Phong,[1,2,3,*,†] Héctor Sainz-Cruz,[4,*,‡] Eugene J. Mele,[1,§] and Francisco Guinea[4,5,‖]

[1]*Department of Physics and Astronomy, University of Pennsylvania, Philadelphia, Pennsylvania 19104, USA*
[2]*Department of Physics, Florida State University, Tallahassee, Florida 32306, USA*
[3]*National High Magnetic Field Laboratory, Tallahassee, Florida 32310, USA*
[4]*IMDEA Nanoscience, Faraday 9, 28049 Madrid, Spain*
[5]*Donostia International Physics Center, Paseo Manuel de Lardizábal 4, 20018 San Sebastián, Spain*

(Received 14 September 2023; revised 18 February 2024; accepted 26 June 2024; published 10 September 2024)

Inspired by recent experimental discoveries of superconductivity in multilayer graphene, we study models of f-wave superconductivity on the honeycomb lattice with arbitrary numbers of layers. For odd numbers of layers, these systems are topologically nontrivial, characterized by a mirror-projected winding number $\nu_{\pm} = \pm 1$. Along each mirror-preserving edge in armchair nanoribbons, there are two protected Majorana zero modes. These modes are present even if the sample is finite in both directions, such as in rectangular and hexagonal flakes. Crucially, zero modes can also be confined to vortex cores. Finally, we apply these models to twisted bilayer and trilayer systems, which also feature boundary-projected and vortex-confined zero modes. Since vortices are experimentally accessible by local scanning probes, our study suggests that superconducting multilayer graphene systems are promising platforms to create and manipulate Majorana zero modes.

DOI: 10.1103/PhysRevB.110.L100501

Due to their non-Abelian braiding statistics and immunity to quantum decoherence, Majorana zero modes (MZMs) are highly sought after as building blocks for topological quantum computation [1–3]. They are believed to exist as excitations of the $\nu = 5/2$ fractional quantum Hall effect [4,5], at the ends of a spinless p-wave superconducting chain [6], or in the vortex cores of spin-triplet $p_x + ip_y$ superconductors [7–9]. However, these platforms are challenging to realize experimentally because a full understanding of the $\nu = 5/2$ state remains elusive while spin-triplet superconductors are scarce in nature [10]. To circumvent these problems, the modern search for MZMs focuses primarily on proximitized systems [11–15], using which various groups claimed to have observed MZMs due to the presence of zero-bias conductance peaks [16–24]. However, it is now clear that disorder-induced Andreev bound states can masquerade as MZMs in conductance experiments [25–32]. Therefore, quenching disorder is an important goal in the pursuit of MZMs.

As an exceptionally low-disorder platform [33,34], graphene is a promising material for the realization of MZMs. Up to now, graphene-based proposals have involved the proximity effect due to the lack of intrinsic superconductivity [35–37]. Several recent groundbreaking experiments shifted this paradigm by showing that graphene multilayers are robust, highly-tunable superconductors [38–48], with mounting evidence suggesting that these states involve an exotic, non-s-wave pairing [43–45,49–52]. In particular, spin-triplet, valley-odd f-wave pairing is emerging as a leading candidate for the superconducting symmetry [49,50,53,54]. Inspired by these recent developments, we study models of *intrinsic* f-wave superconductivity in chirally stacked multilayer graphene. We show that in odd-layer configurations, these systems are topological mirror superconductors characterized by a nontrivial mirror winding number. Therefore, nanoribbons with mirror-symmetric edges *must* host one Majorana mirror pair per boundary. Finite flakes also support zero modes with mirror character and degeneracy determined by the precise termination. Boundary states and their consequences for spectroscopy for the monolayer case were also considered in Refs. [55,56]. Furthermore, we calculate the spectrum of finite flakes that host vortices. We find that a pair of zero modes is confined to each vortex core. This observation holds significant experimental implications since vortices can be readily created and probed by existing techniques [57–65]. Finally, we extend these results to twisted systems, wherein robust zero modes are found in twisted trilayer graphene, but not in twisted bilayer graphene. Importantly, a pair of zero modes is also trapped at vortices in twisted trilayer graphene. Our work suggests that multilayer graphene is an experimentally feasible, ultraclean Majorana platform.

We begin with a simple model of *spinless* superconducting monolayer graphene wherein the superconducting order parameter in real space is described by hoppings between the electrons and holes of the same sublattice with phase winding as indicated in Fig. 1(a). Importantly, the order parameter changes signs between the K and K' valleys, realizing an exotic f-wave superconductor. We will show that at mirror-symmetric boundaries of nanoribbons, this model supports topologically protected pairs of MZMs. The tight-binding

*These authors contributed equally to this work.
†Contact author: vophong@magnet.fsu.edu
‡Contact author: hector.sainz@imdea.org
§Contact author: mele@physics.upenn.edu
‖Contact author: paco.guinea@imdea.org

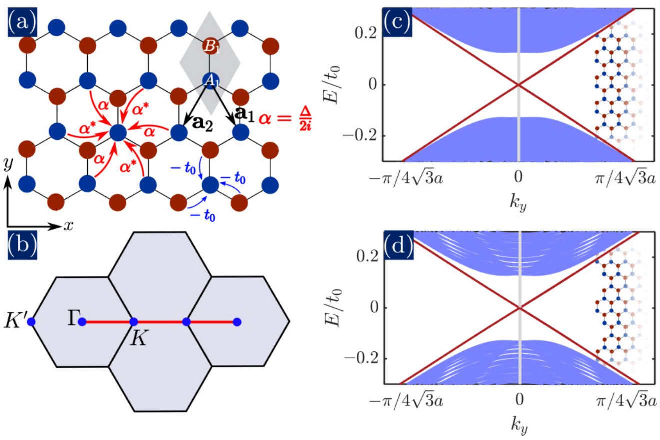

FIG. 1. Majorana zero modes in a monolayer model. (a) Tight-binding model of superconducting monolayer graphene. The hoppings between electrons and electrons (and between holes and holes) are indicated in blue, while the "hoppings" between electrons and holes are indicated in red. (b) The Brillouin zone showing the mirror-symmetric line in red along which the winding number is calculated. (c)–(d) Band structures of mirror-symmetric nanoribbons showing protected edge states that cross zero energy at $k_y = 0$. The edge structures are shown in the insets. Here, $\Delta = \mu = 0.05t_0$, and the ribbons are $99a$ wide.

Hamiltonian is described in Fig. 1(a). The Bogoliubov–de Gennes (BdG) Hamiltonian in momentum space is given by $\hat{\mathcal{H}} = \frac{1}{2}\sum_{\mathbf{k}} \hat{\Psi}^\dagger(\mathbf{k})\mathcal{H}^{\text{BdG}}(\mathbf{k})\hat{\Psi}(\mathbf{k})$, where

$$\begin{aligned}\mathcal{H}^{\text{BdG}}(\mathbf{k}) &= \tau_z[\sigma_0\mu + \sigma_x h_r(\mathbf{k}) - \sigma_y h_i(\mathbf{k})] + \tau_x\sigma_0 g(\mathbf{k}),\\ h(\mathbf{k}) &= h_r(\mathbf{k}) + ih_i(\mathbf{k}) = -t_0(1 + e^{i\kappa_1} + e^{i\kappa_2}),\\ g(\mathbf{k}) &= \Delta[\sin(\kappa_1 - \kappa_2) + \sin(-\kappa_1) + \sin(\kappa_2)], \end{aligned}\tag{1}$$

$\kappa_i = \mathbf{k}\cdot\mathbf{a}_i$, $\mathbf{a}_i$ are the lattice vectors, the τ and σ Pauli matrices act on the Nambu particle-hole and sublattice $\{A, B\}$ spaces respectively with the subscript 0 denoting the identity operator, and $\hat{\Psi}^\dagger(\mathbf{k}) = (\hat{c}^\dagger_{A,\mathbf{k}}, \hat{c}^\dagger_{B,\mathbf{k}}, \hat{c}_{A,-\mathbf{k}}, \hat{c}_{B,-\mathbf{k}})$. This Hamiltonian depends only on three real parameters: $t_0 > 0$ the hopping between nearest neighbors, Δ the superconducting parameter, and μ the chemical potential. Assuming that $\Delta \neq 0$, the bulk band structure is gapped for $|\mu| < t_0$ and $|\mu| > 3t_0$ [66]. We focus only on the lightly-doped regime. Our system respects time reversal $\mathcal{T}$, particle hole $\mathcal{P}$, and mirror $\mathcal{M}_y$ symmetries:

$$\begin{aligned}\mathcal{T} = \tau_z\sigma_0\mathcal{K}: &\quad \mathcal{T}\mathcal{H}^{\text{BdG}}(\mathbf{k})\mathcal{T}^{-1} = \mathcal{H}^{\text{BdG}}(-\mathbf{k}),\\ \mathcal{P} = \tau_x\sigma_0\mathcal{K}: &\quad \mathcal{P}\mathcal{H}^{\text{BdG}}(\mathbf{k})\mathcal{P}^{-1} = -\mathcal{H}^{\text{BdG}}(-\mathbf{k}),\\ \mathcal{M}_y = \tau_0\sigma_x: &\quad \mathcal{M}_y\mathcal{H}^{\text{BdG}}(\mathbf{k})\mathcal{M}_y^{-1} = \mathcal{H}^{\text{BdG}}(\mathcal{M}_y\mathbf{k}),\end{aligned}\tag{2}$$

where $\mathcal{K}$ is the complex conjugation operator. Combining $\mathcal{P}$ and $\mathcal{T}$ leads to a chiral symmetry $\mathcal{C}$:

$$\mathcal{C} = i\tau_y\sigma_0: \quad \mathcal{C}\mathcal{H}^{\text{BdG}}(\mathbf{k})\mathcal{C}^{-1} = -\mathcal{H}^{\text{BdG}}(\mathbf{k}),\tag{3}$$

which requires that every state at $E(\mathbf{k})$ must have a partner at $-E(\mathbf{k})$. Since both $\mathcal{T}^2 = \mathcal{P}^2 = +1$, our system belongs to the topologically trivial two-dimensional BDI class [67]. Therefore, a generic termination does not guarantee the existence of boundary states.

With mirror symmetry, we can enrich the topological classification along mirror-symmetric lines in the Brillouin zone [68–71]. In our case, there is only one independent mirror-symmetric line in the Brillouin zone along $k_y = 0$ as shown in Fig. 1(b) [72]. On this line $[\mathcal{M}_y, \mathcal{H}^{\text{BdG}}(k_x, k_y = 0)] = 0$, so we can block diagonalize the Hamiltonian into a mirror-odd and mirror-even sector. Within each mirror sector, we can further put the Hamiltonian into chiral off-diagonal form since $[\mathcal{M}_y, \mathcal{C}] = 0$ [67,73,74],

$$\mathcal{H}^{\text{BdG}} = \begin{pmatrix}\mathcal{H}_- & 0\\ 0 & \mathcal{H}_+\end{pmatrix}, \quad \text{where} \quad \mathcal{H}_\pm = \begin{pmatrix}0 & \mathcal{D}_\pm\\ \mathcal{D}^\dagger_\pm & 0\end{pmatrix}.\tag{4}$$

The mirror-projected Hamiltonians $\mathcal{H}_\pm$ are characterized by winding numbers $\nu_\pm = \frac{1}{2\pi i}\oint dk_x \text{Tr}[\tilde{\mathcal{D}}^\dagger_\pm(k_x)\partial_{k_x}\tilde{\mathcal{D}}_\pm(k_x)]$, where $\tilde{\mathcal{D}}_\pm(k_x)$ is obtained from $\mathcal{D}_\pm(k_x)$ via singular value decomposition [73,74]. For our model, we have $\mathcal{D}_\pm(k_x) = \mu \pm h(k_x) - ig(k_x)$ and $\nu_\pm = \mp\text{sign}(\Delta/t_0)$. This unity winding number predicts that when a mirror-symmetric edge is cut parallel to the y direction, there exists one topologically protected boundary mode per mirror sector at $k_y = 0$. Importantly, this mode must reside exactly at zero energy due to chiral symmetry. More generally, the odd parity of $\nu_\pm$ guarantees the existence of at least one exact zero mode at $k_y = 0$. We illustrate these zero modes for two mirror-symmetric boundaries in Figs. 1(c)–1(d). In Fig. 1(c), the termination is pristine armchair, while in Fig. 1(d), the termination is jagged armchair that includes both armchair and zigzag characters. In both cases, since $\mathcal{M}_y$ is preserved, we find two zero modes, one from each mirror sector.

The Majorana zero modes can be obtained analytically from a continuum theory for armchair edges. Assuming that $|\Delta|, |\mu| \ll t_0$, the relevant physics is described by a Dirac theory in the original sublattice basis as

$$\mathcal{H}^{\text{BdG}}(\mathbf{r}) = \tau_z[\mu\sigma_0 - i\hbar v_F\nabla_{\mathbf{r}}\cdot(\xi\sigma_x, \sigma_y)] - \xi\tilde{\Delta}\tau_x\sigma_0,\tag{5}$$

where $\hbar v_F = \sqrt{3}t_0 a/2$, $\tilde{\Delta} = 3\sqrt{3}\Delta/2$, and $\xi = \pm$ denotes valley. Putting the edge at $x = 0$ and extending into $x \to -\infty$, the (unnormalized but normalizable) zero-energy solutions at $k_y = 0$ that satisfy the armchair boundary conditions are

$$\psi_{\xi,m_y} = e^{x/\ell - iq_x x}\xi(1, \quad m_y, \quad -im_y\text{sign}\Delta, \quad -i\text{sign}\Delta)^T,\tag{6}$$

where the decay length is $\ell = \hbar v_F/|\tilde{\Delta}|$, the wavelength is $q_x = m_y\xi\mu/\hbar v_F$, and $m_y = \pm 1$ is the mirror eigenvalue of the mode. The valley-antisymmetric nature of the superconducting gap is crucial to the existence of the zero modes in Eq. (6) because had the gap been endowed with the same sign in both valleys, these modes would not have been normalizable. Thus, the presence of armchair-confined Majorana states can serve as a diagnostic of valley-odd, spin-triplet superconductivity in graphene [55]. Away from $k_y = 0$, the mirror-odd and even sectors hybridize, lifting the energy away from zero. To find the dispersion, we can rewrite Eq. (5) at finite small k_y in the basis of Eq. (6)

$$\mathcal{H}^{\text{BdG}}(k_y) = \hbar\tilde{v}_F\begin{pmatrix}0 & ik_y\\ -ik_y & 0\end{pmatrix}.\tag{7}$$

Thus, the mid-gap boundary-projected dispersion is $\mathcal{E} = \pm\hbar\tilde{v}_F k_y$, where $\tilde{v}_F = v_F[1 + (\mu/\tilde{\Delta})^2]^{-1}$, and the associated eigenfunctions are $\psi_{\xi,\mathcal{E}=\pm} = e^{ik_y y}[\mp i\psi_{\xi,m_y=-1} + \psi_{\xi,m_y=+1}]$.

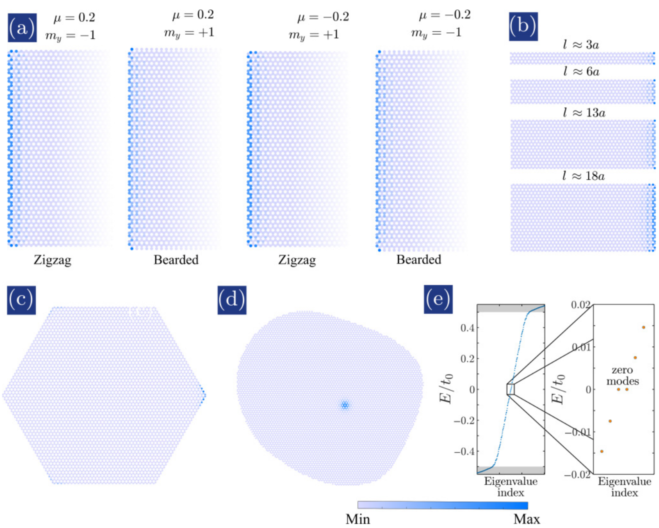

FIG. 2. Isolating Majorana zero modes on finite flakes. (a) Majorana zero mode localized on the left armchair edge of a rectangular flake with different values of the chemical potential and different terminations of the horizontal top and bottom edges (either zigzag or bearded). The mirror eigenvalue of the shown state m_y is indicated. (b) Dependence of the zero mode on vertical length of the flake. (c) Majorana corner state in a hexagonal flake. There are six such states in total. In these simulations, $\Delta = 0.1t_0$ and $|\mu| = 0.2t_0$. (d) One of two vortex states confined to the vortex core near zero energy $E \approx 10^{-17}t_0$, with $\Delta = 0.2t_0$, $\mu = 0.1t_0$, and $d \approx 0$. The irregular shape has 9609 atoms, and is chosen to illustrate that the vortex states do not depend on boundary conditions. The energies of this flake are shown in (e), with the zero modes emphasized. The vortex is centered at a hexagon's center.

For potential applications in topological quantum computing, it is desirable to isolate Majorana zero modes spatially. For our model, the Majorana zero modes always come in pairs as demanded by $\mathcal{M}_y$ along translationally invariant edges. One way to isolate a Majorana zero mode is to break $\mathcal{M}_y$ symmetry by adding a spatially dependent σ_z mass of the form $V(x, y) = m(y)\tau_z\sigma_z$ where $\lim_{y\to\pm\infty} m(y) = \pm m$ and m is a constant. The mass changes sign at $y = 0$. Then, there are two possible zero-energy solutions $\phi_{\xi,m_y} = e^{m_y \int^y m(y')dy'/\hbar v_F}\psi_{\xi,m_y}$ [75]. However, only one of them is normalizable depending on whether m is positive or negative. Thus, the effect of the mirror-breaking mass is to gap out the two boundary modes and create a single bound state localized where the mass changes sign.

Another way to isolate single zero modes is by careful design of edges and corners [56]. For instance, in a rectangular flake that features armchair edges on the left and the right and either zigzag or bearded edges on both the top and the bottom, there are two zero modes that are localized on the left and right armchair edges. These modes are odd (even) under mirror if $\mu > 0$ and the horizontal edges are zigzag (bearded) or if $\mu < 0$ and the horizontal edges are bearded (zigzag), as shown in Fig. 2(a). Therefore, the imposition of zigzag and bearded edges mimics a large σ_z mass above the sample that goes to zero inside the sample and then changes sign below the sample. While the width separating the two armchair edges needs to be large to prevent mixing of the zero modes, the length of the flake along the y direction does not qualitatively affect these modes, as shown in Fig. 2(b). Furthermore, in a hexagonal flake, we find six localized corner states at zero energy, one of which is shown in Fig. 2(c) [56,76]. Spin domain walls can also host pairs of MZMs, see Ref. [77]. It is worth emphasizing that the chosen simulation parameters are unrealistically large to facilitate fast numerical convergence, but should not qualitatively affect the topologically derived conclusions.

Crucially, vortices can also support zero-energy modes. Since vortices break translational symmetry, we calculate these vortex states numerically in real space on finite flakes using the tight-binding framework, where the gap function is modified to $\Delta(\mathbf{r}_i, \mathbf{r}_j) = \pm e^{i\phi_\mathbf{r}}\Delta\tanh(|\mathbf{r}|/d)/2i$, $\mathbf{r} = (\mathbf{r}_i + \mathbf{r}_j)/2$ is the center-of-mass position, $\phi_\mathbf{r}$ is the angular coordinate of $\mathbf{r}$, and d is the coherence length. When the vortex is centered along a $\mathcal{M}_y$-invariant line that connects a hexagon's center and a midbond, we find two vortex-confined modes at numerically exact zero energies, as shown in Fig. 2(d). This is strong evidence that these vortex-confined zero modes are protected by mirror symmetry. When the vortex is centered elsewhere, such as on a carbon site, then these low-energy modes are no longer at zero energy. However, when $d \gtrsim a$, where a is the lattice constant, the precise origin of the vortex becomes less important, and we find near-zero modes for various geometries numerically. The coherence length is the ratio of the Fermi velocity and the superconducting gap, which for practically relevant small gaps, is many times the lattice constant. We leave the topological stability of these modes, including in the presence of disorder, to future analyses.

We now generalize the previous results to rhombohedral N-layer graphene stacks, which is motivated by the recently discovered superconductivity in Bernal bilayer graphene and rhombohedral trilayer graphene [43,45,47,48]. The Hamiltonian is now modified to

$$\mathcal{H}^{\mathrm{BdG}}(\mathbf{k}) = \tau_z\mathcal{H}_N(\mathbf{k}) + \tau_x g(\mathbf{k}), \tag{8}$$

where

$$\mathcal{H}_N(\mathbf{k}) = \mathbb{I}_N\mathcal{H}_{\mathrm{intra}}(\mathbf{k}) + \mathbb{U}_N\mathcal{H}_{\mathrm{inter}}(\mathbf{k}) + \mathbb{L}_N\mathcal{H}^\dagger_{\mathrm{inter}}(\mathbf{k}),$$
$$\mathcal{H}_{\mathrm{intra}}(\mathbf{k}) = \begin{pmatrix} \mu & h(\mathbf{k}) \\ h^*(\mathbf{k}) & \mu \end{pmatrix}, \quad \mathcal{H}_{\mathrm{inter}}(\mathbf{k}) = \begin{pmatrix} 0 & 0 \\ \gamma_1 & 0 \end{pmatrix}, \tag{9}$$

$\mathbb{I}_N$ is the $N \times N$ identity matrix, $\mathbb{U}_N$ ($\mathbb{L}_N$) is the $N \times N$ matrix with ones along the diagonal above (below) the principal diagonal, acting on layer space, and γ_1 is the interlayer hopping. For multiple layers, mirror symmetry is actually $\mathcal{C}_{2x}$ symmetry that simultaneously exchanges layers and sublattices represented by $\mathcal{M}_y = \tau_0\bar{\mathbb{I}}_N\sigma_x$, where $\bar{\mathbb{I}}_N$ is the $N \times N$ *antidiagonal* matrix of ones. For N even, all layers are exchanged under mirror, while for N odd, there is one central layer which is mapped onto itself under mirror. Due to this mirror symmetry, we can classify the bands by the same topological invariant as before. For N even, the system is topologically trivial with $\nu_\pm = 0$. Consequently, there are no Majorana zero modes pinned to $k_y = 0$ on armchair nanoribbons. Interestingly, we find that for the current models, there are still zero modes displaced away from $k_y = 0$. However, it is important to emphasize that these $k_y \neq 0$ modes are *not* topologically protected, and thus they can be removed by perturbations which are invariant under $\mathcal{M}_y$ and do not close the bulk gaps.

One such perturbation is a layer-antisymmetric σ_z potential energy.

On the contrary, for N odd, the systems are topological, protected by $\mathcal{M}_y$, with $\nu_\pm = \pm 1$. Therefore, there are two topological zero modes per armchair edge pinned at $k_y = 0$, in addition to many removable accidental zero modes at nonzero momenta. In addition to these zero modes, we also find numerous midgap states for $N > 1$. Like the nontopological zero modes, these midgap states are also removable; however, they are generically present at armchair edges. The topological zero modes can be removed by breaking $\mathcal{M}_y$. In the multilayer case, one can break $\mathcal{M}_y$ by invalidating layer equivalence with a perpendicular electric field, which is much more experimentally accessible than a staggered potential. Regarding vortices, for the trilayer case, we have also found numerically a number of low-energy states confined to a vortex core. In fact, we find a pair of numerically exact zero modes when the vortex center is located along a $\mathcal{M}_y$-symmetric line. Like before, if $d \gtrsim a$, then the vortex center is not as important, so we find these near-zero modes to be robust. We expect all the odd-layer configurations to feature vortex-confined zero modes, but we have not numerically calculated these due to increasing computational cost.

The above results can be generalized to *ABA* stacks as well. When the number of layers is odd, such a stack can be decomposed into a direct sum of bilayer sectors and one monolayer sector due to the presence of $\mathcal{M}_z$ symmetry [80]. The monolayer sector behaves *exactly* like the monolayer toy model albeit it is written in a basis of a coherent superposition of layers. As such, in these systems, there are also protected Majorana zero modes in the monolayer sector at armchair boundaries and robust vortex-confined low-energy modes. Although superconductivity has not yet been experimentally observed in *ABA* multilayer graphene, these observations suggest that twisted multilayer graphene will contain the same exotic physics owning to the decomposition into a monolayer sector and bilayer sectors.

Inspired by the aforementioned findings, we now look for zero modes in twisted multilayer graphene, using a scaled tight-binding model [53,77,81–87]. Results for twisted bilayer and trilayer graphene appear in Fig. 3. In panel (a), the band structure of a TBG nanoribbon is shown for angle $\theta = 1.06^\circ$, which is close to the magic angle. The bands are qualitatively similar to those of Bernal bilayer graphene. There are 8 zero modes at $k_y \neq 0$, which are *not* topologically protected. These modes and the rest of subgap Andreev states appear near the edges of the system, at the last complete moiré AA regions, as shown in Fig. 3(c), and can be observed via scanning-tunneling microscopy [49,50]. The bands depend sensitively on twist angle. Increasing the angle decreases the momentum of the zero modes. When the angle is increased further, the zero modes disappear and only Andreev states near $k_y = 0$ remain. Few subgap states survive at $\theta \gtrsim 1.2^\circ$ [77].

Just like in TBG, in twisted trilayer graphene (TTG) [41,42], generic $\mathcal{M}_y$-symmetric edges do not lead to topologically protected zero modes at $k_y = 0$. However, a new possibility arises due to the decomposition of TTG into TBG plus monolayer graphene, as found in Ref. [80]. In particular, since the effective monolayer comes from the odd combination of top and bottom layers, when these two layers have

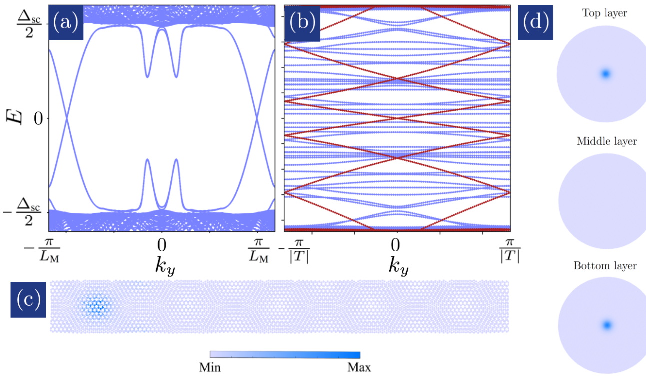

FIG. 3. Twisted multilayer graphene. (a) Band structure of a twisted bilayer graphene nanoribbon, in the hole superconducting dome (filling $n = -2.4$), with a twist angle of $\theta = 1.06^\circ$. The width of the ribbon is $W \approx 35$ moiré periods (L_M) and the superconducting gap is $\Delta_{sc} = 1$ meV. (b) Band structure of a twisted trilayer graphene nanoribbon with armchair edges in the top and bottom layers. The states in red come from the effective monolayer sector and thus have all the charge in top and bottom layers. Here $\theta = 5^\circ$, $\mu = 0$, $\Delta_{sc} = 200$ meV [88], and $|T| > L_M$ due to a commensurability condition [77]. (c) Charge map of a TBG zero mode, showing localization at the last full moiré AA region near an edge. (d) Zero mode confined to a vortex core in twisted trilayer graphene, with $E \approx 10^{-10} t_0$. Here $\theta = 1.5^\circ$, $n = -2.4$, $\Delta_{sc} = 0.05 t_0$, and the flake contains 323 742 atoms.

armchair edges, the system includes the four zero modes at $k_y = 0$, like monolayer graphene, as shown in Fig. 3(b). The charge of these zero modes is indeed evenly distributed in the top and bottom layers, with no charge in the middle layer. Since a decomposition including a monolayer is possible for any alternating-twist stack with an odd number of layers [80], we expect that four zero modes at $k_y = 0$ will exist in all such multilayers. Finally, Fig. 3(d) shows one of the two zero modes confined to a vortex core in twisted trilayer graphene. As in the ribbon geometry, these zero modes come from the effective monolayer sector. These promising results suggest that there is a whole family of robust superconductors in twisted odd-layer graphene that host topologically protected Majorana zero modes.

Superconductivity with f-wave pairing is favored in two-dimensional materials with Fermi pockets at opposing corners of the Brillouin zone and strong repulsive electron-electron interactions. Defects which scatter electrons between the different pockets lead, in the superconducting phase, to Andreev resonances deep within the gap, and even allow for the existence of isolated Majorana states. In particular, the Majorana states are present when $\mathcal{M}_y$ symmetry is respected. This symmetry can be broken by applying a perpendicular displacement field. In rhombohedral stacks, superconductivity has not yet been seen without such a field; so our model might not immediately apply to these cases [43,45,47,48]. However, superconductivity has been unambiguously established in twisted trilayer graphene even in the absence of a displacement field [41,42,89]. Therefore, twisted trilayer graphene is the most promising candidate to detect these Majorana bound states, the observation of which is a simple way to identify this exotic f-wave superconductivity. In these materials, edges and corners are prototypical defects that trap Andreev states and Majorana zero modes. Although precision fabrication of these boundaries is technically challenging, there has been much experimental progress in achieving such a feat [90–94]. On the other hand, vortices are much more experimentally accessible because they can be created in the bulk by a magnetic field or by magnetic impurities. The electronic states at vortex cores have been extensively studied using local probes [57–62]. These techniques can also be used to manipulate vortices [63–65]. Therefore, the vortex-confined zero modes in these graphene-based topological superconductors can be created, probed, and manipulated by readily available technology, opening the way to new types of quantum devices.

We thank Fernando de Juan and Pierre A. Pantaleón for insightful discussions. V.T.P. and E.J.M. are supported by the U.S. Department of Energy under Grant No. DE-FG02-84ER45118. IMDEA Nanociencia acknowledges support from the "Severo Ochoa" Programme for Centres of Excellence in R&D (Grant No. CEX2020-001039-S/AEI/10.13039/501100011033). H.S.-C. and F.G. acknowledge funding from the European Commission, within the Graphene Flagship, Core 3, Grant No. 881603; from Grant No. NMAT2D (Comunidad de Madrid, Spain), SprQuMat, (MAD2D-CM)-MRR MATERIALES AVANZADOS-IMDEA-NC; and from NOVMOMAT, Project No. PID2022-142162NB-I00 funded by Grant No. MICIU/AEI/10.13039/501100011033 and by FEDER, UE.

[1] D. A. Ivanov, Non-Abelian statistics of half-quantum vortices in p-wave superconductors, Phys. Rev. Lett. **86**, 268 (2001).
[2] A. Y. Kitaev, Fault-tolerant quantum computation by anyons, Ann. Phys. **303**, 2 (2003).
[3] C. Nayak, S. H. Simon, A. Stern, M. Freedman, and S. Das Sarma, Non-Abelian anyons and topological quantum computation, Rev. Mod. Phys. **80**, 1083 (2008).
[4] G. Moore and N. Read, Nonabelions in the fractional quantum Hall effect, Nucl. Phys. B **360**, 362 (1991).
[5] N. Read and D. Green, Paired states of fermions in two dimensions with breaking of parity and time-reversal symmetries and the fractional quantum Hall effect, Phys. Rev. B **61**, 10267 (2000).
[6] A. Y. Kitaev, Unpaired Majorana fermions in quantum wires, Phys. Usp. **44**, 131 (2001).
[7] A. Stern, F. von Oppen, and E. Mariani, Geometric phases and quantum entanglement as building blocks for non-Abelian quasiparticle statistics, Phys. Rev. B **70**, 205338 (2004).
[8] S. Das Sarma, C. Nayak, and S. Tewari, Proposal to stabilize and detect half-quantum vortices in strontium ruthenate thin films: Non-Abelian braiding statistics of vortices in a $p_x + ip_y$ superconductor, Phys. Rev. B **73**, 220502(R) (2006).
[9] Y. E. Kraus, A. Auerbach, H. A. Fertig, and S. H. Simon, Majorana fermions of a two-dimensional $p_x + ip_y$ superconductor, Phys. Rev. B **79**, 134515 (2009).
[10] S. Das Sarma, In search of Majorana, Nat. Phys. **19**, 165 (2023).
[11] L. Fu and C. L. Kane, Superconducting proximity effect and Majorana fermions at the surface of a topological insulator, Phys. Rev. Lett. **100**, 096407 (2008).
[12] J. D. Sau, R. M. Lutchyn, S. Tewari, and S. Das Sarma, Generic new platform for topological quantum computation using semiconductor heterostructures, Phys. Rev. Lett. **104**, 040502 (2010).
[13] R. M. Lutchyn, J. D. Sau, and S. Das Sarma, Majorana fermions and a topological phase transition in semiconductor-superconductor heterostructures, Phys. Rev. Lett. **105**, 077001 (2010).
[14] Y. Oreg, G. Refael, and F. von Oppen, Helical liquids and Majorana bound states in quantum wires, Phys. Rev. Lett. **105**, 177002 (2010).
[15] J. Alicea, Majorana fermions in a tunable semiconductor device, Phys. Rev. B **81**, 125318 (2010).
[16] V. Mourik, K. Zuo, S. M. Frolov, S. Plissard, E. P. Bakkers, and L. P. Kouwenhoven, Signatures of Majorana fermions in hybrid superconductor-semiconductor nanowire devices, Science **336**, 1003 (2012).
[17] A. Das, Y. Ronen, Y. Most, Y. Oreg, M. Heiblum, and H. Shtrikman, Zero-bias peaks and splitting in an Al–InAs nanowire topological superconductor as a signature of Majorana fermions, Nat. Phys. **8**, 887 (2012).
[18] M. Deng, C. Yu, G. Huang, M. Larsson, P. Caroff, and H. Xu, Anomalous zero-bias conductance peak in a Nb–InSb nanowire–Nb hybrid device, Nano Lett. **12**, 6414 (2012).
[19] A. D. K. Finck, D. J. Van Harlingen, P. K. Mohseni, K. Jung, and X. Li, Anomalous modulation of a zero-bias peak in a hybrid nanowire-superconductor device, Phys. Rev. Lett. **110**, 126406 (2013).
[20] H. O. H. Churchill, V. Fatemi, K. Grove-Rasmussen, M. T. Deng, P. Caroff, H. Q. Xu, and C. M. Marcus, Superconductor-nanowire devices from tunneling to the multichannel regime: Zero-bias oscillations and magnetoconductance crossover, Phys. Rev. B **87**, 241401(R) (2013).
[21] S. Nadj-Perge, I. K. Drozdov, J. Li, H. Chen, S. Jeon, J. Seo, A. H. MacDonald, B. A. Bernevig, and A. Yazdani, Observation of Majorana fermions in ferromagnetic atomic chains on a superconductor, Science **346**, 602 (2014).
[22] J. Chen, P. Yu, J. Stenger, M. Hocevar, D. Car, S. R. Plissard, E. P. Bakkers, T. D. Stanescu, and S. M. Frolov, Experimental phase diagram of zero-bias conductance peaks in superconductor/semiconductor nanowire devices, Sci. Adv. **3**, e1701476 (2017).
[23] S. Vaitiekėnas, Y. Liu, P. Krogstrup, and C. Marcus, Zero-bias peaks at zero magnetic field in ferromagnetic hybrid nanowires, Nat. Phys. **17**, 43 (2021).
[24] Z. Wang, H. Song, D. Pan, Z. Zhang, W. Miao, R. Li, Z. Cao, G. Zhang, L. Liu, L. Wen, R. Zhuo, D. E. Liu, K. He, R. Shang, J. Zhao, and H. Zhang, Plateau regions for zero-bias peaks within 5% of the quantized conductance value $2e^2/h$, Phys. Rev. Lett. **129**, 167702 (2022).
[25] J. Liu, A. C. Potter, K. T. Law, and P. A. Lee, Zero-bias peaks in the tunneling conductance of spin-orbit-coupled superconducting wires with and without Majorana end-states, Phys. Rev. Lett. **109**, 267002 (2012).

[26] D. Roy, N. Bondyopadhaya, and S. Tewari, Topologically trivial zero-bias conductance peak in semiconductor Majorana wires from boundary effects, Phys. Rev. B **88**, 020502(R) (2013).
[27] J. Chen, B. D. Woods, P. Yu, M. Hocevar, D. Car, S. R. Plissard, E. P. A. M. Bakkers, T. D. Stanescu, and S. M. Frolov, Ubiquitous non-Majorana zero-bias conductance peaks in nanowire devices, Phys. Rev. Lett. **123**, 107703 (2019).
[28] E. Prada, P. San-Jose, M. W. A. de Moor, A. Geresdi, E. J. H. Lee, J. Klinovaja, D. Loss, J. Nygård, R. Aguado, and L. P. Kouwenhoven, From Andreev to Majorana bound states in hybrid superconductor–semiconductor nanowires, Nat. Rev. Phys. **2**, 575 (2020).
[29] H. Pan and S. Das Sarma, Physical mechanisms for zero-bias conductance peaks in Majorana nanowires, Phys. Rev. Res. **2**, 013377 (2020).
[30] H. Pan, C.-X. Liu, M. Wimmer, and S. Das Sarma, Quantized and unquantized zero-bias tunneling conductance peaks in Majorana nanowires: Conductance below and above $2e^2/h$, Phys. Rev. B **103**, 214502 (2021).
[31] S. Das Sarma and H. Pan, Disorder-induced zero-bias peaks in Majorana nanowires, Phys. Rev. B **103**, 195158 (2021).
[32] M. Valentini, M. Borovkov, E. Prada, S. Martí-Sánchez, M. Botifoll, A. Hofmann, J. Arbiol, R. Aguado, P. San-Jose, and G. Katsaros, Majorana-like Coulomb spectroscopy in the absence of zero-bias peaks, Nature (London) **612**, 442 (2022).
[33] N. M. R. Peres, *Colloquium:* The transport properties of graphene: An introduction, Rev. Mod. Phys. **82**, 2673 (2010).
[34] S. Das Sarma, S. Adam, E. H. Hwang, and E. Rossi, Electronic transport in two-dimensional graphene, Rev. Mod. Phys. **83**, 407 (2011).
[35] P. San-Jose, J. L. Lado, R. Aguado, F. Guinea, and J. Fernández-Rossier, Majorana zero modes in graphene, Phys. Rev. X **5**, 041042 (2015).
[36] F. Peñaranda, R. Aguado, E. Prada, and P. San-Jose, Majorana bound states in encapsulated bilayer graphene, SciPost Phys. **14**, (2023).
[37] Y.-M. Xie, E. Lantagne-Hurtubise, A. F. Young, S. Nadj-Perge, and J. Alicea, Gate-defined topological Josephson junctions in Bernal bilayer graphene, Phys. Rev. Lett. **131**, 146601 (2023).
[38] Y. Cao, V. Fatemi, S. Fang, K. Watanabe, T. Taniguchi, E. Kaxiras, and P. Jarillo-Herrero, Unconventional superconductivity in magic-angle graphene superlattices, Nature (London) **556**, 43 (2018).
[39] M. Yankowitz, S. Chen, H. Polshyn, Y. Zhang, K. Watanabe, T. Taniguchi, D. Graf, A. F. Young, and C. R. Dean, Tuning superconductivity in twisted bilayer graphene, Science **363**, 1059 (2019).
[40] X. Lu, P. Stepanov, W. Yang, M. Xie, M. A. Aamir, I. Das, C. Urgell, K. Watanabe, T. Taniguchi, G. Zhang, A. Bachtold, A. H. MacDonald, and D. K. Efetov, Superconductors, orbital magnets and correlated states in magic-angle bilayer graphene, Nature (London) **574**, 653 (2019).
[41] J. M. Park, Y. Cao, K. Watanabe, T. Taniguchi, and P. Jarillo-Herrero, Tunable strongly coupled superconductivity in magic-angle twisted trilayer graphene, Nature (London) **590**, 249 (2021).
[42] Z. Hao, A. M. Zimmerman, P. Ledwith, E. Khalaf, D. H. Najafabadi, K. Watanabe, T. Taniguchi, A. Vishwanath, and P. Kim, Electric field-tunable superconductivity in alternating-twist magic-angle trilayer graphene, Science **371**, 1133 (2021).
[43] H. Zhou, T. Xie, T. Taniguchi, K. Watanabe, and A. F. Young, Superconductivity in rhombohedral trilayer graphene, Nature (London) **598**, 434 (2021).
[44] J. M. Park, Y. Cao, L.-Q. Xia, S. Sun, K. Watanabe, T. Taniguchi, and P. Jarillo-Herrero, Robust superconductivity in magic-angle multilayer graphene family, Nat. Mater. **21**, 877 (2022).
[45] H. Zhou, L. Holleis, Y. Saito, L. Cohen, W. Huynh, C. L. Patterson, F. Yang, T. Taniguchi, K. Watanabe, and A. F. Young, Isospin magnetism and spin-polarized superconductivity in Bernal bilayer graphene, Science **375**, 774 (2022).
[46] Y. Zhang, R. Polski, C. Lewandowski, A. Thomson, Y. Peng, Y. Choi, H. Kim, K. Watanabe, T. Taniguchi, J. Alicea, F. von Oppen, G. Refael, and S. Nadj-Perge, Promotion of superconductivity in magic-angle graphene multilayers, Science **377**, 1538 (2022).
[47] Y. Zhang, R. Polski, A. Thomson, É. Lantagne-Hurtubise, C. Lewandowski, H. Zhou, K. Watanabe, T. Taniguchi, J. Alicea, and S. Nadj-Perge, Enhanced superconductivity in spin–orbit proximitized bilayer graphene, Nature (London) **613**, 268 (2023).
[48] L. Holleis, C. L. Patterson, Y. Zhang, H. M. Yoo, H. Zhou, T. Taniguchi, K. Watanabe, S. Nadj-Perge, and A. F. Young, Ising superconductivity and nematicity in Bernal bilayer graphene with strong spin orbit coupling, arXiv:2303.00742.
[49] M. Oh, K. P. Nuckolls, D. Wong, R. L. Lee, X. Liu, K. Watanabe, T. Taniguchi, and A. Yazdani, Evidence for unconventional superconductivity in twisted bilayer graphene, Nature (London) **600**, 240 (2021).
[50] H. Kim, Y. Choi, C. Lewandowski, A. Thomson, Y. Zhang, R. Polski, K. Watanabe, T. Taniguchi, J. Alicea, and S. Nadj-Perge, Evidence for unconventional superconductivity in twisted trilayer graphene, Nature (London) **606**, 494 (2022).
[51] J.-X. Lin, P. Siriviboon, H. D. Scammell, S. Liu, D. Rhodes, K. Watanabe, T. Taniguchi, J. Hone, M. S. Scheurer, and J. Li, Zero-field superconducting diode effect in small-twist-angle trilayer graphene, Nat. Phys. **18**, 1221 (2022).
[52] Y. Cao, J. M. Park, K. Watanabe, T. Taniguchi, and P. Jarillo-Herrero, Pauli-limit violation and re-entrant superconductivity in moiré graphene, Nature (London) **595**, 526 (2021).
[53] H. Sainz-Cruz, P. A. Pantaleón, V. T. Phong, A. Jimeno-Pozo, and F. Guinea, Junctions and superconducting symmetry in twisted bilayer graphene, Phys. Rev. Lett. **131**, 016003 (2023).
[54] V. Crépel, T. Cea, L. Fu, and F. Guinea, Unconventional superconductivity due to interband polarization, Phys. Rev. B **105**, 094506 (2022).
[55] T. H. Kokkeler, C. Huang, F. S. Bergeret, and I. V. Tokatly, Spectroscopic signature of spin triplet odd-valley superconductivity in two-dimensional materials, Phys. Rev. B **108**, L180504 (2023).
[56] R. Ghadimi, S. H. Lee, and B.-J. Yang, Boundary-obstructed topological superconductor in buckled honeycomb lattice under perpendicular electric field, Phys. Rev. B **107**, 224511 (2023).
[57] H. Suderow, I. Guillamón, J. G. Rodrigo, and S. Vieira, Imaging superconducting vortex cores and lattices with a scanning tunneling microscope, Supercond. Sci. Technol. **27**, 063001 (2014).
[58] C. Berthod, I. Maggio-Aprile, J. Bruér, A. Erb, and C. Renner, Observation of Caroli–de Gennes–Matricon

vortex states in $YBa_2Cu_3O_{7-\delta}$, Phys. Rev. Lett. **119**, 237001 (2017).

[59] L. Kong, S. Zhu, M. Papaj, H. Chen, L. Cao, H. Isobe, Y. Xing, W. Liu, D. Wang, P. Fan, Y. Sun, S. Du, J. Schneeloch, R. Zhong, G. Gu, L. Fu, H.-J. Gao, and H. Ding, Half-integer level shift of vortex bound states in an iron-based superconductor, Nat. Phys. **15**, 1181 (2019).

[60] X. Chen, W. Duan, X. Fan, W. Hong, K. Chen, H. Yang, S. Li, H. Luo, and H.-H. Wen, Friedel oscillations of vortex bound states under extreme quantum limit in $KCa_2Fe_4As_4F_2$, Phys. Rev. Lett. **126**, 257002 (2021).

[61] T. Zhang, W. Bao, C. Chen, D. Li, Z. Lu, Y. Hu, W. Yang, D. Zhao, Y. Yan, X. Dong, Q.-H. Wang, T. Zhang, and D. Feng, Observation of distinct spatial distributions of the zero and nonzero energy vortex modes in $(Li_{0.84}Fe_{0.16})OHFeSe$, Phys. Rev. Lett. **126**, 127001 (2021).

[62] C. Li, Y.-F. Zhao, A. Vera, O. Lesser, H. Yi, S. Kumari, Z. Yan, C. Dong, T. Bowen, K. Wang, H. Wang, J. L. Thompson, K. Watanabe, T. Taniguchi, D. R. Hickey, Y. Oreg, J. A. Robinson, C.-Z. Chang, and J. Zhu, Proximity-induced superconductivity in epitaxial topological insulator/graphene/gallium heterostructures, Nat. Mater. **22**, 570 (2023).

[63] J.-Y. Ge, V. N. Gladilin, J. Tempere, C. Xue, J. T. Devreese, J. V. de Vondel, Y. Zhou, and V. V. Moshchalkov, Nanoscale assembly of superconducting vortices with scanning tunnelling microscope tip, Nat. Commun. **7**, 13880 (2016).

[64] H. Polshyn, T. Naibert, and R. Budakian, Manipulating multivortex states in superconducting structures, Nano Lett. **19**, 5476 (2019).

[65] T. R. Naibert, H. Polshyn, R. Garrido-Menacho, M. Durkin, B. Wolin, V. Chua, I. Mondragon-Shem, T. Hughes, N. Mason, and R. Budakian, Imaging and controlling vortex dynamics in mesoscopic superconductor–normal-metal–superconductor arrays, Phys. Rev. B **103**, 224526 (2021).

[66] The latter condition is trivially true because it simply corresponds to fully filled or fully empty fermionic bands.

[67] C.-K. Chiu, J. C. Y. Teo, A. P. Schnyder, and S. Ryu, Classification of topological quantum matter with symmetries, Rev. Mod. Phys. **88**, 035005 (2016).

[68] F. Zhang, C. L. Kane, and E. J. Mele, Topological mirror superconductivity, Phys. Rev. Lett. **111**, 056403 (2013).

[69] F. Zhang, C. L. Kane, and E. J. Mele, Time-reversal-invariant topological superconductivity and Majorana Kramers pairs, Phys. Rev. Lett. **111**, 056402 (2013).

[70] Y. Ueno, A. Yamakage, Y. Tanaka, and M. Sato, Symmetry-protected Majorana fermions in topological crystalline superconductors: Theory and application to Sr_2RuO_4, Phys. Rev. Lett. **111**, 087002 (2013).

[71] K. Shiozaki and M. Sato, Topology of crystalline insulators and superconductors, Phys. Rev. B **90**, 165114 (2014).

[72] It may appear that there are two mirror-symmetric lines: one along $k_y = 0$ and one along $k_y = 2\pi/\sqrt{3}a$, but these two are actually connected to each other by a reciprocal lattice vector. So they are *not* independent.

[73] T. Neupert and F. Schindler, Topological crystalline insulators, in *Topological Matter: Lectures from the Topological Matter School 2017*, edited by D. Bercioux, J. Cayssol, M.G. Vergniory, and M. Reyes Calvo (Springer International Publishing, Cham, 2018), pp. 31–61.

[74] L. Lin, Y. Ke, and C. Lee, Real-space representation of the winding number for a one-dimensional chiral-symmetric topological insulator, Phys. Rev. B **103**, 224208 (2021).

[75] We continue to label the ϕ_{ξ,m_y} states with mirror eigenvalue m_y only as a matter of convenience. The reader should *not* take this as implying that mirror symmetry is preserved. It is indeed broken explicitly by the potential $V(x, y)$.

[76] The hexagonal shape can be thought of as an example of the rule that most clean, locally straight graphene edges are described, in the continuum limit, by the zigzag boundary conditions. This arises from the fact that the projection of the K and K' points on the edge only coincide (realizing the armchair boundary conditions) for very specific angles between the edges and the lattice axes [95]. Edge regions connecting A- and B-like boundaries must include armchairlike segments, where zero modes will be localized. Examples of zero modes in a distorted hexagon are shown in Ref. [77].

[77] See Supplemental Material at http://link.aps.org/supplemental/10.1103/PhysRevB.110.L100501 for derivations of all the models reported in the main text and additional supporting results, which includes Refs. [78] and [79].

[78] C.-K. Chiu, H. Yao, and S. Ryu, Classification of topological insulators and superconductors in the presence of reflection symmetry, Phys. Rev. B **88**, 075142 (2013).

[79] D. A. Abanin, P. A. Lee, and L. S. Levitov, Spin-filtered edge states and quantum Hall effect in graphene, Phys. Rev. Lett. **96**, 176803 (2006).

[80] E. Khalaf, A. J. Kruchkov, G. Tarnopolsky, and A. Vishwanath, Magic angle hierarchy in twisted graphene multilayers, Phys. Rev. B **100**, 085109 (2019).

[81] L. A. Gonzalez-Arraga, J. L. Lado, F. Guinea, and P. San-Jose, Electrically controllable magnetism in twisted bilayer graphene, Phys. Rev. Lett. **119**, 107201 (2017).

[82] X. Lin and D. Tománek, Minimum model for the electronic structure of twisted bilayer graphene and related structures, Phys. Rev. B **98**, 081410(R) (2018).

[83] J. Vahedi, R. Peters, A. Missaoui, A. Honecker, and G. T. de Laissardière, Magnetism of magic-angle twisted bilayer graphene, SciPost Phys. **11**, 083 (2021).

[84] H. Sainz-Cruz, T. Cea, P. A. Pantaleón, and F. Guinea, High transmission in twisted bilayer graphene with angle disorder, Phys. Rev. B **104**, 075144 (2021).

[85] F. Guinea and N. R. Walet, Electrostatic effects, band distortions, and superconductivity in twisted graphene bilayers, Proc. Natl. Acad. Sci. **115**, 13174 (2018).

[86] R. Bistritzer and A. H. MacDonald, Moiré bands in twisted double-layer graphene, Proc. Natl. Acad. Sci. **108**, 12233 (2011).

[87] P. Moon, Y.-W. Son, and M. Koshino, Optical absorption of twisted bilayer graphene with interlayer potential asymmetry, Phys. Rev. B **90**, 155427 (2014).

[88] This twist angle and superconducting gap are not realistic for TTG and are chosen only to facilitate the convergence of the computation.

[89] Y. Cao, J. M. Park, K. Watanabe, T. Taniguchi, and P. Jarillo-Herrero, Large Pauli limit violation and reentrant superconductivity in magic-angle twisted trilayer graphene, arXiv:2103.12083.

[90] J. Cai, P. Ruffieux, R. Jaafar, M. Bieri, T. Braun, S. Blankenburg, M. Muoth, A. P. Seitsonen, M. Saleh, X. Feng *et al.*, Atomically precise bottom-up fabrication of graphene nanoribbons, Nature (London) **466**, 470 (2010).

[91] L. Talirz, P. Ruffieux, and R. Fasel, On-surface synthesis of atomically precise graphene nanoribbons, Adv. Mater. **28**, 6222 (2016).

[92] P. Ruffieux, S. Wang, B. Yang, C. Sánchez-Sánchez, J. Liu, T. Dienel, L. Talirz, P. Shinde, C. A. Pignedoli, D. Passerone *et al.*, On-surface synthesis of graphene nanoribbons with zigzag edge topology, Nature (London) **531**, 489 (2016).

[93] T. Kitao, M. W. MacLean, K. Nakata, M. Takayanagi, M. Nagaoka, and T. Uemura, Scalable and precise synthesis of armchair-edge graphene nanoribbon in metal–organic framework, J. Am. Chem. Soc. **142**, 5509 (2020).

[94] R. K. Houtsma, J. de la Rie, and M. Stöhr, Atomically precise graphene nanoribbons: Interplay of structural and electronic properties, Chem. Soc. Rev. **50**, 6541 (2021).

[95] A. R. Akhmerov and C. W. J. Beenakker, Boundary conditions for Dirac fermions on a terminated honeycomb lattice, Phys. Rev. B **77**, 085423 (2008).